Chinese Chemical Letters 36 (2025) 110259

Contents lists available at ScienceDirect

Chinese Chemical Letters

journal homepage: www.elsevier.com/locate/cclet

Design of host-guest interaction based molecularly imprinted polymers: Targeting recognition of the epitope of neuron-specific enolase *via* a SERS assay

Ran Zhu, Pan Zhang, Yitong Xu, Jiutong Ma, Qiong Jia*

College of Chemistry, Jilin University, Changchun 130012, China

ARTICLE INFO

Article history:
Received 9 May 2024
Revised 12 July 2024
Accepted 15 July 2024
Available online 15 July 2024

Keywords:
Molecularly imprinted polymers
Host-guest interaction
Oriented epitope imprinting
Surface-enhanced Raman scattering
Neuron-specific enolase

ABSTRACT

Molecularly imprinted polymers (MIPs) are a kind of synthetic receptors possessing wide application prospects in proteins recognition. However, there are still great challenges in proteins imprinting due to their large size and easy conformation change. In this study, we explored epitope-oriented MIP based on host-guest interaction (hg-MIP) and constructed a novel hg-MIP-SERS (surface-enhanced Raman scatting) approach for efficiently recognizing the terminal epitopes of neuron-specific enolase (NSE), a well-known disease biomarker for small cell lung cancer, neuroblstom, and Alzheimer's disease. The C- and N-terminal epitopes of NSE were modified with 4-(phenylazo) benzoic acid, then they were used as the templates and immobilized on β-cyclodextrin-functionalized substrates. The imprinted layer was formed by polymerization of various functional monomers. Combined with SERS detection, an antibody-free sandwich assay based on hg-MIP was successfully used to detect the concentration of NSE in human serums, with the advantages of simple operation, small sample volume (5 μL), wide linear range (1–10^4 ng/mL) and a limit of detection as low as 0.01 ng/mL. The developed epitope-oriented hg-MIP-SERS approach can also be extended to other proteins, expanding the imprinting method of proteins, and has a broad development space in the field of protein separation and detection.

Many diseases arise from the structural change and aberrant expression of intracellular proteins. Thus, quite a lot of proteins have been routinely employed as disease biomarkers for early clinical diagnosis [1,2]. At present, mass spectrometry [3], fluorescence [4,5], and surface-enhanced Raman scattering (SERS) [6-8] are main methods to determine protein biomarkers. However, the detection of trace amount proteins from real biological samples with various interfering substances remains challenging and high-selectivity recognition methods are indispensable to achieve precise isolation and enrichment of proteins from complex samples.

Molecularly imprinted polymers (MIPs) are synthetic receptors which have the characteristics of selective molecular recognition, high stability, simple preparation, reusability and low cost [9-13], and have been used as antibody alternatives in immunoassay [14]. Recently, the employment of MIPs for the recognition of specific proteins has obtained increasing attention [15-17]. Nevertheless, proteins are bulky and conformationally unstable and some proteins are unable to be used as templates on account of their high price and difficult availability, so the protein imprinting still poses great challenges [18,19].

Epitope surface imprinting materials has been diffusely used owing to its advantage of high template removal rate and great accessibility to target proteins [20,21]. There are two important steps for epitope surface imprinting, *i.e.*, immobilizing the epitope template on the surface of the solid substrate and forming a thin imprinting layer around the template. The first step is extremely important to make the recognition sites uniform and improve the binding efficiency of MIPs [22]. The intrinsic functional groups on the amino acids are commonly used for immobilization, yet this tends to cause inconsistent epitopes orientation [23]. Recently, some oriented epitope imprinting methods have been explored [22,24]. Although some progresses have been made in epitope-oriented approaches, it is still an urgent need to explore facile and universal approaches for oriented epitope immobilization.

Host-guest interaction has the characteristics of being dynamic and reversible [25,26], based on which some platforms have been opened up for the construction of stimulus-responsive and sensitive materials [27,28] including our previous work [29,30]. Among them, the host-guest interaction of β-cyclodextrin (β-CD) and

* Corresponding author.
E-mail address: jiaqiong@jlu.edu.cn (Q. Jia).

https://doi.org/10.1016/j.cclet.2024.110259
1001-8417/

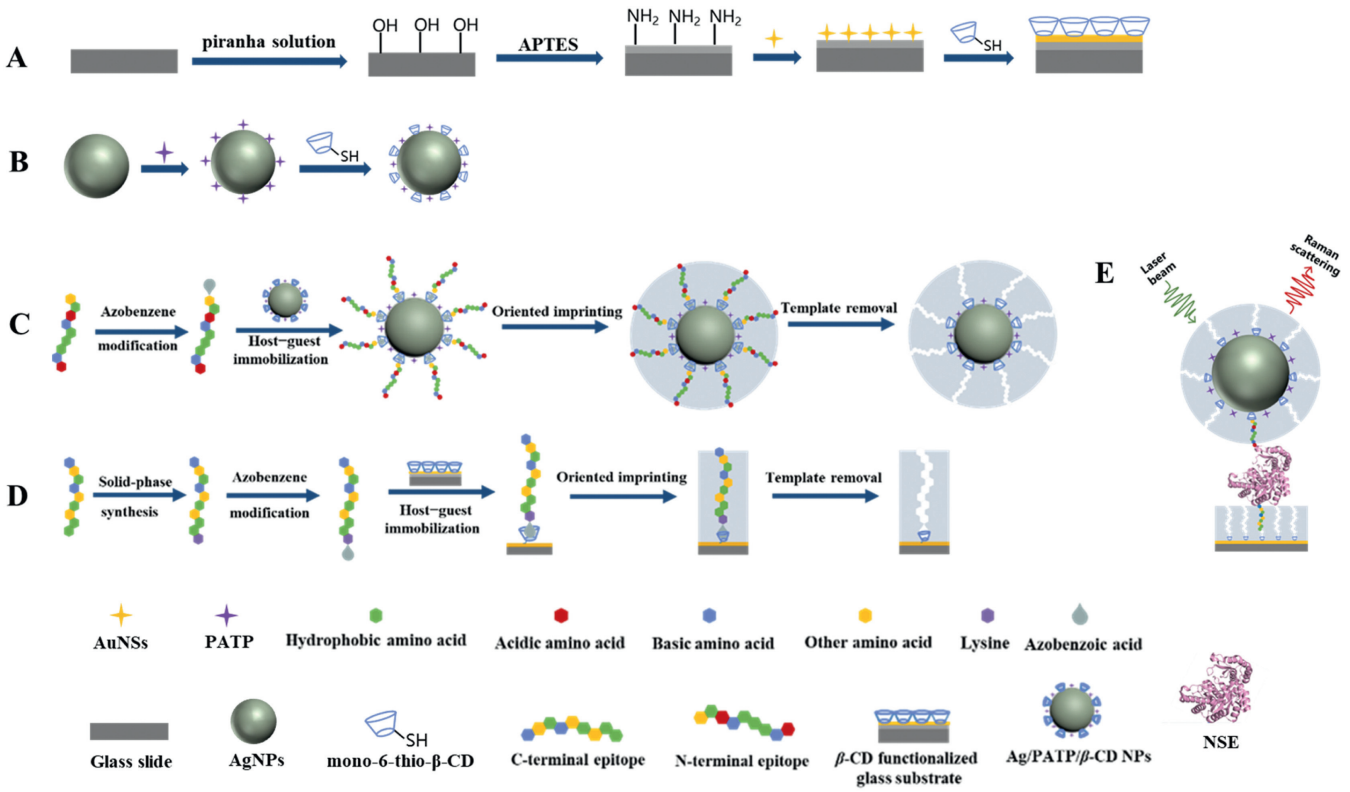

Scheme 1. Schematic illustration of (A) β-CD functionalized glass substrates, (B) Ag/PATP/β-CD NPs, (C) N-terminal epitope-imprinted AgNPs, and (D) C-terminal epitope-imprinted glass substrate. (E) hg-MIP-SERS approach for the detection of NSE.

azobenzene (Azo) has been highly favored since its discovery by virtue of the high molecular recognition and reversible assembly and disassembly under light stimulation [30-34]. Azo can be reversibly converted between *trans* and *cis* by alternating irradiation with visible (vis) and ultraviolet (UV) light [35,36]. *Trans*-Azo can combine with the cavity of β-CD to form 1:1 inclusion complex, which assists epitope template with suitable orientation. Under the irradiation of UV, *trans*-Azo is isomerized to *cis*-Azo, which can slip out quickly from the cavity of β-CD because of its mismatch with the cavity size of β-CD [37].

Herein, we developed a strategy for the preparation of epitope-oriented host-guest interaction based MIP (hg-MIP) and constructed a novel hg-MIP-SERS approach. The procedure and principle of this imprinting method are shown in Scheme 1. C- and N-terminal peptides of neuron-specific enolase (NSE), which is the disease biomarker for small cell lung cancer (SCLC), neuroblstom, and Alzheimer's disease [38], was selected as the epitopes in this work. Lysine and 4-(phenylazo)benzoic acid were in turn attached to C-terminal peptide while N-terminal peptide was first-hand modified with 4-(phenylazo)benzoic acid to get Azo modified template epitopes. Azo modified C- and N-terminal epitopes were severally immobilized onto two kinds of substrates by means of host-guest interaction, namely β-CD functionalized glass substrates and β-CD/*p*-amino-thiophenol (PATP, Raman reporter) functionalized Ag nanoparticles (AgNPs). Then the imprinting layer was formed by polymerization of various silanylation reagents. Finally, the imprinting templates were removed under the action of UV irradiation and eluent to obtain C-terminal epitope-imprinted glass plate and N-terminal epitope-imprinted AgNPs. The C-terminal epitope-imprinted glass plate was used for target capturing in complex samples, while N-terminal epitope-imprinted AgNPs were used as Raman labeling nanotags. After the target protein was captured and labeled, sandwich-like immunocomplexes were formed. Meanwhile, Raman-active nanotags fell into the hotspot, which was achieved at the gap between C-terminal epitope-imprinted glass plate and N-terminal epitope-imprinted AgNPs due to plasmonic coupling, and thus the generated Raman signal was further enhanced [39]. This hg-MIP-SERS method was successfully used to determine NSE in the serum samples from SCLC patient and healthy people. The developed approach can also be extended to other proteins, endowing hg-MIP-SERS with broad application prospects in the field of protein detection and disease diagnosis.

Transmission electron microscopy (TEM) was utilized to expresses the morphology of the synthesized gold nanostars (AuNSs) (Fig. S2A in Supporting information), indicating that AuNSs are three-dimensional branched nanoparticles with star morphology. In previous studies, AuNSs were reported as splendid SERS nanosubstrates, where much higher SERS enhancement than the Au nanosphere can be observed [40]. This is due to the fact that the extremely small radii of curvature and surface plasmons originating from the hybridization of individual tips and cores result in strong electric field enhancement [41-43]. The UV–vis absorption spectrum (Fig. S2B in Supporting information) displays two surface plasmon resonance peaks at 518 and 658 nm, respectively. The latter is the longitudinal plasmon resonance while the former is the transverse plasmon of the tip [44,45]. These results suggest that negatively charged AuNSs were successfully synthesized in *N*-(2-hydroxyethyl)piperazine-*N*′-(2-ethanesulfonic acid) (HEPES) buffer solution, which can be immobilized on positively charged glass sheets by electrostatic interaction. This approach can be easily conducted in a common laboratory without complex equipment, which has advantages in commercial production. Scanning electron microscopy (SEM) images of AuNSs self-assembled glass plate and C-terminal epitope-imprinted glass plate are shown in Figs. S2C and D (Supporting information). AuNSs were well organized in the glass plate, while the surface of the glass sheet is smoother af-

ter the polymerization of the functional monomers, indicating that the imprinting process is successful. The chemical composition of AuNSs self-assembled glass plate, glass plate immobilized with Azo modified C-terminal epitopes, and C-terminal epitope-imprinted glass plate was compared using X-ray photoelectron spectroscopy (XPS) analysis. As presented in Fig. S3A (Supporting information), the peaks of O 1s, N 1s, C 1s, Si 2p, and Au 4f appear in the spectrum of AuNSs self-assembled glass plate. After immobilizing Azo modified C-terminal epitopes, the peak of N 1s is significantly enhanced. In addition, XPS high-resolution spectra of C 1s and O 1s of Azo modified C-terminal epitopes and C-terminal epitope-imprinted glass plate are displayed in Figs. S3B–E (Supporting information). The peaks corresponding to C-N and C-O appear owing to the introduction of functional monomers (Fig. S3D in Supporting information) [31]. As for O 1s, the appearance of new peak referring to Si-O-H indicates the successful formation of the imprinting layer (Fig. S3E in Supporting information) [46].

The surface water contact angles (CA) were employed to measure the hydrophilicity of the obtained glass plate during the synthesis process. As illustrated in Fig. S4 (Supporting information), CA degrees of glass plate after cleaning with piranha solution, AuNSs self-assembled glass plate, β-CD modified glass plate, and C-terminal epitope-imprinted glass plate are 33°, 69°, 43°, and 71°, respectively. The surface of the cleaned glass plate is rich in hydroxyl groups and has good hydrophilicity (Fig. S4A). After assembling negatively charged AuNSs onto the glass surface, water molecules cannot form a smooth contact with the uneven material surface, resulting in a larger CA (Fig. S4B). As for β-CD modified glass plate, the hydrophilic surface of β-CD leads to a decrease in CA (Fig. S4C). In the contrast, the abundant alkyl groups in the imprinting layer increase the hydrophobicity, and thus the CA of C-terminal epitope-imprinted glass plate is larger (Fig. S4D). These results fully demonstrate the success of each modification step.

TEM images show the morphologies of AgNPs and N-terminal epitope-imprinted AgNPs (Figs. S5A and B in Supporting information). Comparing AgNPs with N-terminal epitope-imprinted AgNPs, the imprinting layer is clearly visible, and the thickness of the imprinting layer is about 4 nm. The extinction spectra of AgNPs, Ag/PATP/β-CD NPs, and N-terminal epitope-imprinted AgNPs were studied (Fig. S6 in Supporting information). The absorption intensity of Ag/PATP/β-CD NPs decreases slightly because of the adsorption of PATP and β-CD to AgNPs through Ag-S bond. The aggregation of particles results in a significant broadening of the absorption peak after imprinting. Fig. S7 (Supporting information) shows Raman spectra of AgNPs, Ag/PATP NPs, Ag/PATP/β-CD-Azo-N-terminal epitope NPs, and N-terminal epitope-imprinted AgNPs. Raman peaks are contributed from 4,4-dimercaptoazo-benzene (DMAB) generated by the photocatalytic coupling reaction of PATP (Fig. S8 in Supporting information) on AgNPs under laser irradiation during SERS measurement [47-49]. The attributions of the main Raman peaks are displayed in Table S1 (Supporting information). The signals at 1390 and 1435 cm^{-1} in Raman spectrum are N=N stretching mode of DMAB. After the formation of the imprinting layer, the intensity of these two peaks decreases significantly, which also indicates that the imprinting process was successfully realized. 1435 cm^{-1} was selected for subsequent quantitative analysis in this experiment.

To achieve high recognition performance of the developed hg-MIP, the imprinting conditions including the proportion of functional monomers and imprinting time were optimized according to imprinting factor (*IF*), which is the ratio of the amount of prepared MIP and nonimprinted polymer (NIP)-captured templates. The length of Azo modified C-terminal epitopes was calculated on the basis of Chem 3D simulation (Fig. S9A in Supporting information) and its length is approximately 4.53 nm. According to the relationship between the thickness and imprinting time previously established by Liu's group [22], $y = (0.066 \pm 0.003)x + (0.161 \pm 0.183)$ ($R^2 = 0.988$), the imprinting time of C-terminal was set at 50, 60, 70, and 80 min. As illustrated in Figs. S10A-C, the highest *IF* value of 3.20 was obtained when the proportion of APTES/UBTES/IBTES/TEOS is 10:20:20:50 and the imprinting time is 70 min. Compared with controllable oriented surface imprinting of boronate affinity-anchored epitopes proposed by Liu *et al.*'s report [47], the difference in C-terminal nonapeptide modification method does not affect the choice of functional monomer ratio, so 10:10:20:60 was selected as the ratio of functional monomers for N-terminal imprinting.

Thus, only the imprinting time needs to be considered when optimizing N-terminal imprinting conditions. The length of Azo modified N-terminal epitope was also simulated by Chem 3D (Fig. S9B in Supporting information), which is about 4.24 nm. The imprinting time was set to 40, 50, 60, and 70 min. It can be seen from Fig. S10D (Supporting information) that the highest *IF* value (8.12) was obtained at imprinting time of 60 min. The thickness of the imprinted layer gained under this imprinting condition is 4 nm (Fig. S5B in Supporting information), which is in line with the simulated length.

The specificity of epitope-oriented hg-MIP was studied by matrix assisted laser desorption/ionization time of flight mass spectrometer (MALDI-TOF MS). The enzymatic hydrolysates of horseradish peroxidase (HRP) and bovine serum albumin (BSA) were added into the standard solutions of C-terminal or N-terminal peptides, and the mixture was enriched with the prepared MIP and NIP, respectively. As shown in Fig. S11 (Supporting information), a lot of competing peptides were detected before extraction. After enrichment by the synthesized MIP, the interferences were almost removed and only C-terminal or N-terminal peptides were detected. In contrast, almost no peptides were detected after enrichment with NIP, indicating that the synthesized C- and N-terminal imprinted polymers offer well-formed cavity with complementary shape and size to the target, and the developed hg-MIP possesses good specificity at the peptide level. The basis for the specific binding between antibodies and antigens is the special arrangement of several amino acids on the surface of proteins, and the epitope imprinting materials simulate this recognition site, thus possess high specificity for target proteins. Furthermore, the overall selectivity of hg-MIP-SERS was examined with NSE as the target protein and HRP, transferrin (TRF), BSA, and ovalbumin (OVA). The extraction time and labeling time were selected according to previous reported literature [47]. As presented in Fig. S12 (Supporting information), this hg-MIP-SERS method possesses excellent selectivity.

As displayed in Fig. 1A, Raman spectra of NSE within the concentration range from 10 pg/mL to 100 μg/mL were detected. Raman intensity at 1435 cm^{-1} increases with NSE concentrations. The adsorption isotherms of MIP and NIP were studied by plotting intensity at 1435 cm^{-1} against the logarithm of NSE concentrations (Fig. 1B). For hg-MIP-SERS, Raman intensity increases linearly with the increase of NSE concentration in the range of 1 ng/mL–10 μg/mL ($y = 725.68x - 1219.82$, $R^2 = 0.995$), which was used as the linear calibration curves for quantitative analysis. Progressive disease can be effectively indicated by NSE in SCLC [50] and this range satisfies the requirements demanded in clinical applications. The limit of detection (LOD) is 10 pg/mL (1.3×10^{-13} mol/L) (signal-to-noise ratio, S/N = 4). For NIP-SERS, Raman intensity does not apparently increase with the increase of NSE concentrations. These results demonstrate that the imprinting procedure is efficient. Table S2 (Supporting information) summarizes the reported methods for NSE detection in view of MIPs. The current method does not need antibodies and has the advantage of wide linear range and low LOD, indicating its great potential for identifying NSE. Moreover, the binding constant (K_d) was investigated by fit-

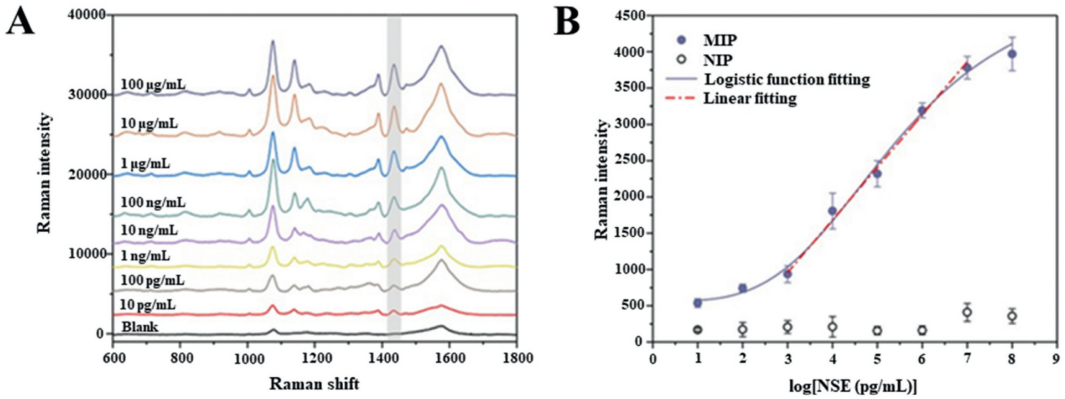

Fig. 1. (A) Raman spectra for NSE at different concentrations detected by hg-MIP-SERS and (B) Dependence of Raman intensity at 1435 cm^{-1} gained by hg-MIP-SERS and NIP-SERS on logarithm of NSE concentrations. The error bars represent the standard deviation for three parallel experiments.

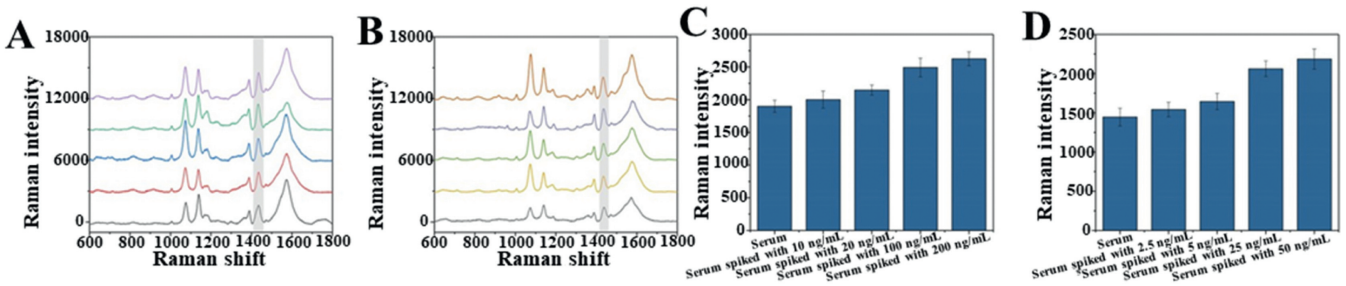

Fig. 2. Raman spectra for (A) SCLC patient and (B) healthy people serum spiked with different concentrations of NSE. Raman intensity at 1435 cm^{-1} for (C) SCLC patient and (D) healthy people serum spiked with different concentrations of NSE. The error bars represent the standard deviation for three parallel experiments.

ting data according to logistic function. K_d was measured as 4.1×10^{-9} mol/L, suggesting the good affinity of the obtained MIP.

The stability of MIPs is a feature superior to that of natural antibodies. The prepared hg-MIP was stored for a period of time before used to detect NSE. Results are demonstrated in Fig. S13 (Supporting information), illustrating that even after storage for 60 days at the temperature of 4 °C, Raman intensity remains 89% of the freshly synthesized materials, which demonstrates the excellent stability of the developed hg-MIP. In addition, the developed hg-MIP can be utilized three times without significant loss in the binding capacity for NSE.

To demonstrate the utility of the developed hg-MIP-SERS method, it was used to measure the concentration of NSE in real human serum samples. In this study, it can be assumed that the prepared MIP can effectively eliminate matrix effect owing to the highly specific of the prepared hg-MIP for NSE. The concentrations of NSE in the serums of SCLC patient and healthy people were counted to be 19.95 and 4.68 ng/mL according to linear calibration curve, respectively. To verify the validity of these results, a series of spiked serum samples containing known NSE concentrations (c_i) were determined by this hg-MIP-SERS method [51]. Fig. 2 displays the obtained Raman spectra and Raman intensity at 1435 cm^{-1} of serum samples. The measured Raman intensity at 1435 cm^{-1} was plotted against the logarithm of the total concentration of NSE ($c_0 + c_i$) in the spiked samples (Fig. S14 in Supporting information), where c_0 was calculated according to the linear equation obtained with standard solutions. The fitting curves of two serum samples both conform to a good linear relationship (for SCLC patient, $y = 720.65x–1196.31$, $R^2 = 0.989$; for healthy people, $y = 734.30x - 1268.59$, $R^2 = 0.987$), which are close to the linear calibration curve. Therefore, this assumption is reasonable and the calculated concentrations of the unlabeled samples are acceptable.

Furthermore, commercial enzyme-linked immunosorbent assays (ELISA) kit was utilized to detect the concentrations of NSE in the above-mentioned human serum samples. Table S3 (Supporting information) illustrates the comparison for the two results, which demonstrates no significance difference. This suggests that the hg-MIP-SERS method is feasible for practical application. As summarized in Table S3, the current method possesses some merits such as wider linear range, lower LOD, lower sample volume compared with ELISA kit.

In brief, we developed a novel epitope-oriented hg-MIP approach, which utilizes host-guest interaction to achieve template immobilization and release by modifying Azo at the end of the epitopes. The synthesized hg-MIP can selectively enrich C- or N-terminal peptides from the peptide mixtures, and combined with SERS to establish a rapid protein detection method. This method was successfully used to detect the concentration of NSE in human serum samples. Compared with traditional immunological method, the current method has the advantages of small sample consumption, wide linear range, and low cost. The controllable epitope-oriented hg-MIP-SERS method can be extended to other proteins, which expands the approach of protein imprinting.

Ethical statement

This study strictly adhered to the principles of Helsinki Declaration and was approved by the Ethics Committee of China-Japan Hospital, Jilin University. In addition, all volunteers and patients who participated in this work agreed to provide serum samples for the study.

Declaration of competing interest

The authors declare that they have no known competing financial interests or personal relationships that could have appeared to influence the work reported in this paper.

CRediT authorship contribution statement

Ran Zhu: Writing – original draft, Visualization, Formal analysis, Data curation. **Pan Zhang:** Writing – original draft, Methodology, Investigation, Conceptualization. **Yitong Xu:** Writing – review & editing, Data curation. **Jiutong Ma:** Writing – review & editing, Supervision. **Qiong Jia:** Writing – review & editing, Supervision, Project administration.

Acknowledgments

This work was financially supported by Open Project of State Key Laboratory of Supramolecular Structure and Materials, Jilin University, China (No. sklssm2024018).

Supplementary materials

Supplementary material associated with this article can be found, in the online version, at doi:10.1016/j.cclet.2024.110259.

References

[1] B. Zhao, W. Xu, J. Ma, Q. Jia, Chin. Chem. Lett. 34 (2023) 107498.
[2] H. Qi, L. Jiang, Q. Jia, Chin. Chem. Lett. 32 (2021) 2629–2636.
[3] X. Zhao, S. Zheng, Y. Li, et al., Anal. Chem. 92 (2020) 690–698.
[4] E. Csibra, G.-B. Stan, Nat. Commun. 13 (2022) 6600.
[5] N.N. Wang, H. Gao, Y.Z. Li, et al., Angew. Chem. Int. Ed. 60 (2021) 197–201.
[6] P. Zhang, G. Chen, Z. Wang, J. Ma, Q. Jia, Sens. Actuator. B: Chem. 361 (2022) 131669.
[7] E. Turan, A. Zengin, Z. Suludere, N.Ö. Kalkan, U. Tamer, Talanta 237 (2022) 122926.
[8] X. Zhang, T. Gan, Z. Xu, et al., Talanta 271 (2024) 125630.
[9] K. Haupt, P.X.M. Rangel, B.T.S. Bui, Chem. Rev. 120 (2020) 9554–9582.
[10] M. Dinc, C. Esen, B. Mizaikoff, TrAC-Trends Anal. Chem. 114 (2019) 202–217.
[11] L. Chen, X. Wang, W. Lu, X. Wu, J. Li, Chem. Soc. Rev. 45 (2016) 2137–2211.
[12] S. Xu, L. Wang, Z. Liu, Angew. Chem. Int. Ed. 60 (2021) 3858–3869.
[13] C. Wu, T. Li, D. Li, et al., Chin. Chem. Lett. 32 (2021) 2174–2178.
[14] J. Pang, P. Li, H. He, S. Xu, Z. Liu, Chem. Sci. 13 (2022) 4589–4597.
[15] Y. Lv, Y. Qin, F. Svec, T. Tan, Biosens. Bioelectr. 80 (2016) 433–441.
[16] M. Dabrowski, P. Lach, M. Cieplak, W. Kutner, Biosens. Bioelectr. 102 (2018) 17–26.
[17] A. Incel, I.A. Diez, C. Wierzbicka, et al., Anal. Chem. 93 (2021) 3857–3866.
[18] E. Verheyen, J.P. Schillemans, M. van Wijk, et al., Biomaterials 32 (2011) 3008–3020.
[19] S. Ansari, S. Masoum, TrAC-Trends Anal. Chem. 114 (2019) 29–47.
[20] K. Yang, S. Li, L. Liu, et al., Adv. Mater. 31 (2019) 1902048.
[21] J. Drzazgowska, B. Schmid, R.D. Suessmuth, Z. Altintas, Anal. Chem. 92 (2020) 4798–4806.
[22] R. Xing, Y. Ma, Y. Wang, Y. Wen, Z. Liu, Chem. Sci. 10 (2019) 1831–1835.
[23] Y.T. Qin, H. Peng, X.W. He, W.Y. Li, Y.K. Zhang, Anal. Chem. 91 (2019) 12696–12703.
[24] S. Li, K. Yang, J. Liu, et al., Anal. Chem. 87 (2015) 4617–4620.
[25] P. Li, Z. Li, D. Zhang, Q. Jia, Chin. Chem. Lett. 34 (2023) 107619.
[26] W. Ji, Y. Wang, H. Zhang, et al., Chromatographia 86 (2023) 469–482.
[27] H. Yang, B. Yuan, X. Zhang, O.A. Scherman, Acc. Chem. Res. 47 (2014) 2106–2115.
[28] B. Zhao, L. Jiang, Q. Jia, Chin. Chem. Lett. 32 (2021) 2629–2636.
[29] H. Zheng, X. Li, Q. Jia, ACS Appl. Mater. Interfaces 10 (2018) 5909–5917.
[30] H. Zheng, Z. Wang, Q. Jia, Small Methods 7 (2023) 2300254.
[31] Q. Bian, W. Wang, S. Wang, G. Wang, ACS Appl. Mater. Interfaces 8 (2016) 27360–27367.
[32] X. Zhou, C. Wang, Z. Wang, et al., Biosens. Bioelectr. 148 (2020) 111810.
[33] J. Zheng, Y. Nie, S. Yang, et al., Anal. Chem. 86 (2014) 10208–10214.
[34] J. Gao, Z. Guo, F. Su, et al., Biosens. Bioelectr. 63 (2015) 465–471.
[35] X.Y. Zhao, X.Q. Fang, S.J. Yang, et al., Carbohydr. Polym. 251 (2021) 10.
[36] S. Cai, B. Luo, P. Jiang, et al., Nanoscale 10 (2018) 14280–14289.
[37] J.A. Krings, B. Vonhoeren, P. Tegeder, et al., J. Mater. Chem. A 2 (2014) 9587–9593.
[38] S.K. Arya, S. Bhansali, Chem. Rev. 111 (2011) 6783–6809.
[39] L. Zhou, Y. Wang, R. Xing, et al., Biosens. Bioelectron. 145 (2019) 111729.
[40] M. Li, S.K. Cushing, J. Zhang, et al., Nanotechnology 23 (2012) 115501.
[41] A. Indrasekara, S. Meyers, S. Shubeita, et al., Nanoscale 6 (2014) 8891–8899.
[42] M. Arabi, A. Ostovan, Z. Zhang, et al., Biosens. Bioelectr. 174 (2021) 112825.
[43] Y. Wang, B. Yan, L. Chen, Chem. Rev. 113 (2013) 1391–1428.
[44] J. Xie, J.Y. Lee, D.I.C. Wang, Chem. Mater. 19 (2007) 2823–2830.
[45] W. Xi, A.J. Haes, J. Am. Chem. Soc. 141 (2019) 4034–4042.
[46] Y.L. Khung, S.H. Ngalim, A. Scaccabarozzi, D. Narducci, Beilstein J. Nanotech. 6 (2015) 19–26.
[47] R. Xing, Y. Wen, Y. Dong, et al., Anal. Chem. 91 (2019) 9993–10000.
[48] D.Y. Wu, L.B. Zhao, X.M. Liu, et al., Chem. Commun. 47 (2011) 2520–2522.
[49] Y.F. Huang, H.P. Zhu, G.K. Liu, et al., J. Am. Chem. Soc. 132 (2010) 9244–9246.
[50] W. Ebert, M. Hoppe, T. Muley, P. Drings, Anticancer Res. 17 (1997) 2875–2878.
[51] X. Tu, P. Muhammad, J. Liu, et al., Anal. Chem. 88 (2016) 12363–12370.